ELSEVIER

Chemical Engineering Journal 135S (2008) S21–S29

Chemical Engineering Journal

www.elsevier.com/locate/cej

A numerical study on a *macroscopic* Stokes number based on shear-induced interparticle collisions in a micro-separator/classifier

Shinichi Ookawara [a,*], David Street [b], Kohei Ogawa [a]

[a] *Department of Chemical Engineering, Tokyo Institute of Technology, Tokyo 152-8552, Japan*
[b] *Fluent Asia Pacific, Tokyo 160-0023, Japan*

Abstract

In the present study a *macroscopic* Stokes number Stk_s is newly proposed for efficient operation of a micro-separator/classifier. The Stk_s is a ratio of particle relaxation time to interval of shear-induced interparticle collisions. The collision interval is estimated based on a representative shear rate and average particle concentration passing through an outer plane defined at the end of arc microchannel. The device efficiency is evaluated in terms of reduced particle recovery R_c to the outer plane. It is shown that the Stk_s would be useful for predicting a maximum feed concentration to be handled with a highest R_c.

Keywords: Microstructure; Particle separation/classification; Collision; Stokes number; Lift force

1. Introduction

The micro-separator/classifier under consideration is a novel microfluidic device [1], whose functional component is an arc microchannel. A series of experimental and numerical studies have confirmed that the principle for particle separation is entirely due to both the curvature and size of the channel [2–9]. As the channel size is reduced, but keeping the geometry and Reynolds number constant, then by definition the average velocity through the channel increases. As a result, both shear rate and centrifugal acceleration become large as they are both inversely proportional to the squared and cubed power of the size, respectively. The large shear rate makes the lift-force effect dominant in the microchannel, whereas it is usually negligible in larger devices. When the shear rate is large enough compared to the particle size, the velocities are rather different even at both sides of a microsphere. Such velocity differences around the particle bring about the large lift force so that particles migrate to a region of higher velocity. On the other hand, the large centrifugal force shifts the higher velocity region towards the outer wall of the arc microchannel. Consequently, the particles contained in a slurry are concentrated near the outer wall. A bifurcation at the end of the arc section is used to separate or classify the particles in the slurry. It has been confirmed that a device size that could bring about this function has the width, depth and arc radius of 100–400 μm, 75–200 μm and 10–20 mm, respectively. The superiority of the micro-separator/classifier has been experimentally proven in terms of separation sharpness and energy efficiency compared with existing large device, such as a hydrocyclone [4,7].

Fig. 1 schematically shows how particles are concentrated near the outer wall at the downstream of arc microchannel based on a previous study [6]. The figure also depicts the assumption that the flow vertically split at the arc end would develop into flows passing through inner and outer branches of the actual device [5]. In this study, accordingly, the inner and outer planes are examined at the arc end instead of inner and outer branches for evaluating particle recovery as a device performance. It can be readily understood that the particle recovery to the outer plane much depends on the particle concentration profile and where to split the arc-end plane. As the flow rate in the outer branch is decreased keeping total flow-rate constant in the main channel, for instance, the split position shifts outwards and the outer plane accordingly becomes smaller. Consequently, a certain amount of particles would undesirably report to the inner branch. It is apparent that the outer flow-rate should be controlled taking into account the concentration profile. On the other hand, the previous study predicted that the ratio of maximum to feed concentrations at the arc end decreased beyond a critical feed concentration while it remained constant in the dilute conditions. The decrease of the ratio implies that the concentration profile becomes flat and then the particle recovery to the outer plane

* Corresponding author. Tel.: +81 3 5734 3035; fax: +81 3 5734 2882.
E-mail address: sokawara@chemeng.titech.ac.jp (S. Ookawara).

1385-8947/$ – see front matter © 2007 Elsevier B.V. All rights reserved.
doi:10.1016/j.cej.2007.07.016

Nomenclature

C_e	C^* normalized by C^* obtained at the most dilute condition
C^*	a ratio of maximum to feed particle concentrations at the arc-end plane
d_p	particle diameter (m)
D_h	hydraulic diameter of rectangular channel (m)
$\mathbf{F}_{Lift,f}$	reaction force of $\mathbf{F}_{Lift,p}$ (N/m^3)
$\mathbf{F}_{Lift,p}$	lift force acting on the particle (N/m^3)
$\mathbf{g}$	gravity (m/s^2)
K	exchange coefficient (kg/m^3 s)
p, p_s	pressure and solid pressure (Pa)
R	particle recovery to outer plane or branch
Re	Reynolds number
R_c	reduced particle recovery
$R_{c,dilute}$	R_c obtained at the most dilute condition
R_f	fluid recovery to outer plane
S	shear rate (1/s)
Stk	Stokes number = ratio of particle relaxation time to collision interval
Stk_s	Stokes number based on shear-induced collisions from *macroscopic* viewpoint
$Stk_{s,micro}$	Stokes number based on shear-induced collisions from microscopic viewpoint
$\mathbf{u}$	fluid velocity (m/s)
U	mean velocity in main channel (m/s)
$\mathbf{v}$	particle velocity (m/s)
w	mass flow rate (kg/s)

Greek symbols

α	volume fraction
μ	viscosity (Pa s)
ρ	density (kg/m^3)
τ_c	collision interval between particles (s)
τ_p	particle relaxation time (s)
$\underline{\underline{\tau}}$	stress–strain tensor (Pa)

Subscripts

f, p	fluid and particle
feed	feed
in, out	inner and outer planes

would decline. Further, it was found that the concentrated region expanded beyond the limit. The expansion beyond the split position also suggests that more particles flow into the inner branch inadequately. Both the phenomena would interactively decrease the particle recovery. It is of a practical interest, therefore, to identify the critical feed concentration according to the outer flow-rate for the device operation with a highest efficiency.

In the previous study, it was interpreted that interparticle collisions due to the high shear rate brought about those undesirable phenomena, viz., flattening and expanding of particle concentration profiles. Consequently, a novel Stokes number was introduced for predicting the onset of the phenomena taking into account the shear-induced collisions. Generally, Stokes number Stk is defined as a ratio of particle relaxation time $\tau_p = \{(\rho_p + \rho_f/2)d_p^2\}/(18\mu_f)$ to the interval of interparticle collisions τ_c as:

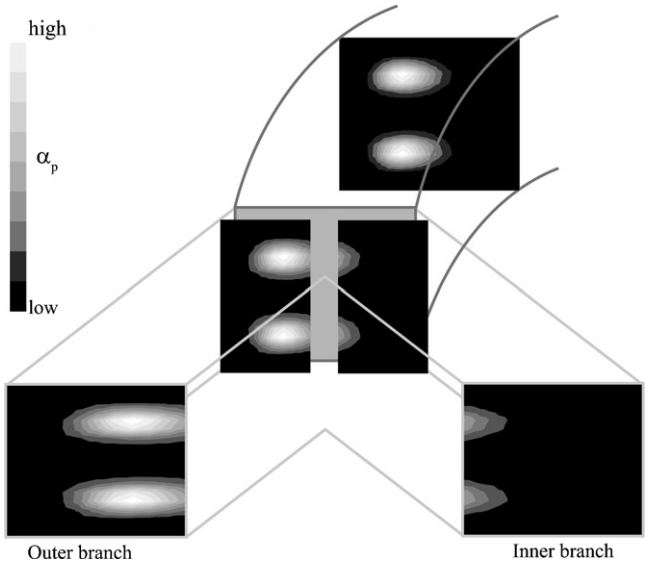

Fig. 1. A schematic diagram of developed particle concentration profile at the downstream of arc microchannel and vertical split of the flow at the arc end leading to particle recovery from the outer branch of the bifurcation.

$$Stk = \frac{\tau_p}{\tau_c} \tag{1}$$

When Stk is much smaller than unity, particle motion is governed by fluid flow by means of drag and lift force acting on the particle, that is, the particle follows the fluid motion with little slip velocity while the interval of the particle collision is so large that the collisions do not affect the particle motion. In this case, the slurry is regarded as dilute. On the other hand, when Stk is much larger than unity, particle inertia is so large that fluid motion does not affect the particle behavior while frequent collisions, whose intervals are short, do influence the particle motion. In this case, slurry can be regarded as dense [10,11].

Accordingly, simple concentration definitions such as particle volume or weight fraction cannot alone be used to characterize whether a slurry is dilute or dense. In the study of micro-separator/classifiers, the particle relaxation time is considerably small as tens of microseconds because of the particle size and density. On the other hand, the extremely high shear rate, which is indispensable to achieve particle separation/classification by a curved microchannel, could cause interparticle collisions even within such a short relaxation time. The particles could have enough relative velocity within the scale of particle diameter due to the high shear rate so that particles can frequently collide with each other. Since the collisions disperse the particles over the channel, a dense slurry with $Stk \gg 1$ cannot be separated with a high efficiency. In our previous study, the collision interval due to the shear rate was locally evaluated as

$$\tau_c = \frac{\pi}{8\alpha_p S} \tag{2}$$

where α_p and S are the local particle volume fraction and shear rate in solid phase over the arc-end plane [6]. The microscopic Stokes number $Stk_{s,micro}$ based on the shear-induced particle collisions was then defined as:

$$Stk_{s,micro} = \frac{4\alpha_p(\rho_p + \rho_f/2)d_p^2 S}{9\pi\mu_f} \quad (3)$$

Since this value can be evaluated locally (at a point) anywhere over the cross-sectional plane at the arc end, the maximum value was taken as a representative value for the given conditions. On the other hand, the concentration effect C^* was defined as a maximum particle concentration at the arc end divided by the feed concentration. To examine the feed concentration effect on C^*, a concentration efficiency C_e was defined as C^* obtained at a given feed concentration normalized by C^* obtained at the most dilute feed concentration. It is expected that C_e remains at unity in the dilute range where particle collisions are negligible, viz., $Stk_{s,micro} \ll 1$. It was confirmed that the decline of C_e began at $Stk_{s,micro}$ of 0.1 and the trend could be correlated with $Stk_{s,micro}$ regardless of the particle size.

Although this finding was really useful for understanding the characteristics of the micro-separator/classifier, the $Stk_{s,micro}$ cannot be utilized directly for practical operation. Those local indices were evaluated because of the employed numerical approach, viz., Euler-granular model that treats both liquid and solid as interpenetrating continuous phases. In practical operation, however, these values cannot be measured by any means.

In order to establish a practical operation, therefore, a *macroscopic* Stokes number Stk_s is newly proposed using the values experimentally available. The local shear rate found somewhere over the plane will be substituted by a representative shear rate defined based on mean velocity and hydraulic diameter of the main arc channel. Instead of the local particle concentration, evaluated is an average particle concentration of the slurry passing through the outer plane. The validity of these substitutions will be discussed based on the profiles of velocity and particle concentration. Instead of the C_e defined at a point over the plane, further, a reduced particle recovery R_c to the outer plane is evaluated as a device performance since the reduced particle recovery to the outer branch is utilized in practical operation. The relation between the Stk_s and R_c is examined at three representative split positions in the feed concentration range of 0.0006–0.15 for 10 and 20 μm particles.

2. Numerical methods and *macroscopic* Stokes number

2.1. Numerical methods

In the previous study [6], particle concentration profiles in the arc microchannel were modeled at Reynolds number of 450 in the feed concentration range of 0.0006–0.15 by means of the Euler-granular model implemented in a commercial CFD code [12]. Based on the results, the relation between microscopic (local) Stokes number $Stk_{s,micro}$ and the concentration efficiency C_e was discussed. Although the discussion was useful to understand the characteristic of the micro-separator/classifier, those defined indices were not available experimentally. In the present study, therefore, the numerical solutions are re-analyzed from a *macroscopic* viewpoint to find a new relation between indices that can be obtained experimentally.

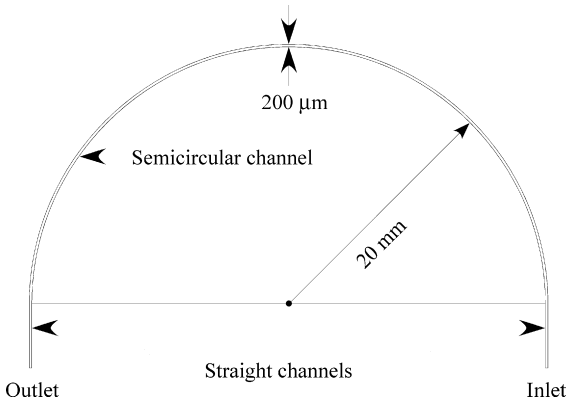

Fig. 2. A schematic diagram of the geometry used for simulation.

Here, the numerical methods are briefly summarized since the details were given in the previous work. Fig. 2 schematically shows the geometry for the simulation. The width and depth of the rectangular channels are 200 and 170 μm, respectively. The radius of the main semicircular section is 20 mm. These sizes are identical to the dimensions of the first prototype examined in experiments [1]. The bifurcation at an arc end is not modeled and both the ends are connected to straight channels with a length of 5 mm. The density ρ_f and viscosity μ_f of water, defined as continuous phase, are 1000 kg/m^3 and 0.001 Pa s, respectively. The density ρ_p of the dispersed phase is specified as 1190 kg/m^3. Monodisperse spherical particles whose diameters d_p are 10 and 20 μm are examined in each numerical simulation.

The governing equations to be solved are as follows:

Conservation of mass:

Fluid phase:

$$\nabla \cdot (\alpha_f \mathbf{u}) = 0 \quad (4)$$

Particulate phase:

$$\nabla \cdot (\alpha_p \mathbf{v}) = 0 \quad (5)$$

where α_f and α_p denote the volume fractions of fluid and particulate phases, and $\mathbf{u}$ and $\mathbf{v}$ are the velocities of fluid and particle, respectively.

Conservation of momentum:

Fluid phase:

$$-\nabla \cdot (\alpha_f \rho_f \mathbf{uu}) - \alpha_f \nabla p + \nabla \cdot \underline{\underline{\tau_f}} + \alpha_f \rho_f \mathbf{g} + K(\mathbf{v} - \mathbf{u}) + \mathbf{F}_{Lift,f} = 0 \quad (6)$$

Particulate phase:

$$-\nabla \cdot (\alpha_p \rho_p \mathbf{vv}) - \alpha_p \nabla p - \nabla p_s + \nabla \cdot \underline{\underline{\tau_p}} + \alpha_p \rho_p \mathbf{g} + K(\mathbf{u} - \mathbf{v}) + \mathbf{F}_{Lift,p} = 0 \quad (7)$$

where $\underline{\underline{\tau_f}}$ and $\underline{\underline{\tau_p}}$ are the stress–strain tensors of fluid and particle.

$$\underline{\underline{\tau_f}} = \alpha_f \mu_f (\nabla \mathbf{u} + \nabla \mathbf{u}^T) \tag{8}$$

$$\underline{\underline{\tau_p}} = \alpha_p \mu_p (\nabla \mathbf{v} + \nabla \mathbf{v}^T) \tag{9}$$

Here μ_f and μ_p represent shear viscosities of fluid and particulate phases. The gravity $\mathbf{g}$ is specified as 9.8 m/s^2 in the perpendicular direction to the plane of the semicircle.

In this study, the lift force acting on the particle $\mathbf{F}_{Lift,p}$ is computed as follows:

$$\mathbf{F}_{Lift,p} = 0.5 \rho_f \alpha_p (\mathbf{u} - \mathbf{v}) \times (\nabla \times \mathbf{u}) \tag{10}$$

The equation is derived assuming inviscid continuous phase, but originally with minus sign [13]. The sign of Drew–Lahey model was reversed as Eq. (10) so that the acting direction became the same as that of the Saffman's lift force [14]. It was confirmed that the lift force model (Eq. (10)) predicted particle concentration profiles at the end of the semicircular section that correspond well with the experimental results [3]. The fluid experiences the force of the same magnitude, but in the opposite direction as

$$\mathbf{F}_{Lift,f} = -\mathbf{F}_{Lift,p} \tag{11}$$

At the inlet to the straight section of the microchannel a uniform velocity U is assumed so that fluid phase Reynolds number is 450. The same velocity U is specified as the inlet boundary condition of the particulate phase. The granular temperature for the solid phase is specified as zero at the inlet. The discussion on the granular temperature is described elsewhere [15] as well as in the previous study. The feed volume fraction $\alpha_{p,feed}$ is varied within the range of 0.0006–0.15. Although particle agglomeration is not particularly considered in the Euler-granular model, it is reasonably assumed that the particles are well dispersed due to the extremely high shear rate even in the denser conditions. The no-slip condition is applied on the channel walls. For the pressure–velocity coupling and discretization schemes for convection terms, the phase-coupled SIMPLE algorithm [16] with a second-order upwind scheme is adopted. For volume fraction, a second-order upwind scheme is employed.

2.2. Reduced particle recovery

Fig. 3 illustrates typical particulate-phase profiles of (a) volume fraction and (b) axial velocity over the arc-end plane for 10 μm particles. The left edge of each contour map corresponds to the outer wall of the arc channel. The Euler-granular calculation also gives the volume fraction and velocity profiles of the liquid phase. These profiles immediately enable one to evaluate the mass flow rates of particulate and liquid phases passing through any bounded plane as follows:

$$w_p = \int_{plane} \rho_p \alpha_p \mathbf{v} \cdot \mathrm{d}s, \qquad w_f = \int_{plane} \rho_f \alpha_f \mathbf{u} \cdot \mathrm{d}s \tag{12}$$

In this study, the cross-sectional plane at the arc end is divided into inner and outer planes typically as shown in Fig. 3. The inner plane represents the conditions of the mixture that flows through the inner exhaust branch of the device and vice versa. The particulate mass flow rates passing through these inner and outer planes, $w_{p,in}$ and $w_{p,out}$ can be used to define a particle recovery R as follows:

$$R = \frac{w_{p,out}}{w_{p,in} + w_{p,out}} \tag{13}$$

The fluid recovery R_f is also given based on the liquid mass flow rates passing through the inner and outer planes, $w_{f,in}$ and $w_{f,out}$.

$$R_f = \frac{w_{f,out}}{w_{f,in} + w_{f,out}} \tag{14}$$

The reduced particle recovery R_c, which is generally utilized as the performance index of hydrocyclones, is calculated for each examined particle size, viz., 10 and 20 μm and in the volume fraction range of 0.0006–0.15 as follows:

$$R_c = \frac{R - R_f}{1 - R_f} \tag{15}$$

The R_c can be regarded as a *macroscopic* separation efficiency of the device, which is also experimentally obtained. The splitting plane methodology to evaluate the reduced particle recovery was validated based on experimental results [5].

2.3. Macroscopic Stokes number

The *macroscopic* Stokes number Stk_s based on shear-induced particle collisions is also defined as:

$$Stk_s = \frac{\tau_p}{\tau_c} \tag{16}$$

where τ_p and τ_c are the particle relaxation time and the particle collision interval, respectively. The τ_p is calculated from fluid and particle properties such as densities, viscosity and diameter as:

$$\tau_p = \frac{(\rho_p + \rho_f/2) d_p^2}{18 \mu_f} \tag{17}$$

In order to evaluate a *macroscopic* collision interval near the outer wall, on the other hand, the particle volume fraction and shear rate in Eq. (2) should be carefully chosen. In this study, the *macroscopic* τ_c is defined as:

$$\tau_c = \frac{\pi D_h}{64 \alpha_{p,out} U} \tag{18}$$

where $\alpha_{p,out}$ is an average particle volume fraction in a slurry passing through the outer plane, which can be obtained as:

$$\alpha_{p,out} = \frac{w_{p,out}/\rho_p}{w_{p,out}/\rho_p + w_{f,out}/\rho_f} \tag{19}$$

Since it is assumed that $\alpha_{p,out}$ corresponds to the particle volume fraction flowing in the outer exhaust branch, the value can be evaluated in experiments by measuring an absorbance of slurry discharged from the outer branch [1].

The numerical estimation is based on the assumption that the $\alpha_{p,out}$ is nearly same as the concentration in the outer wall region

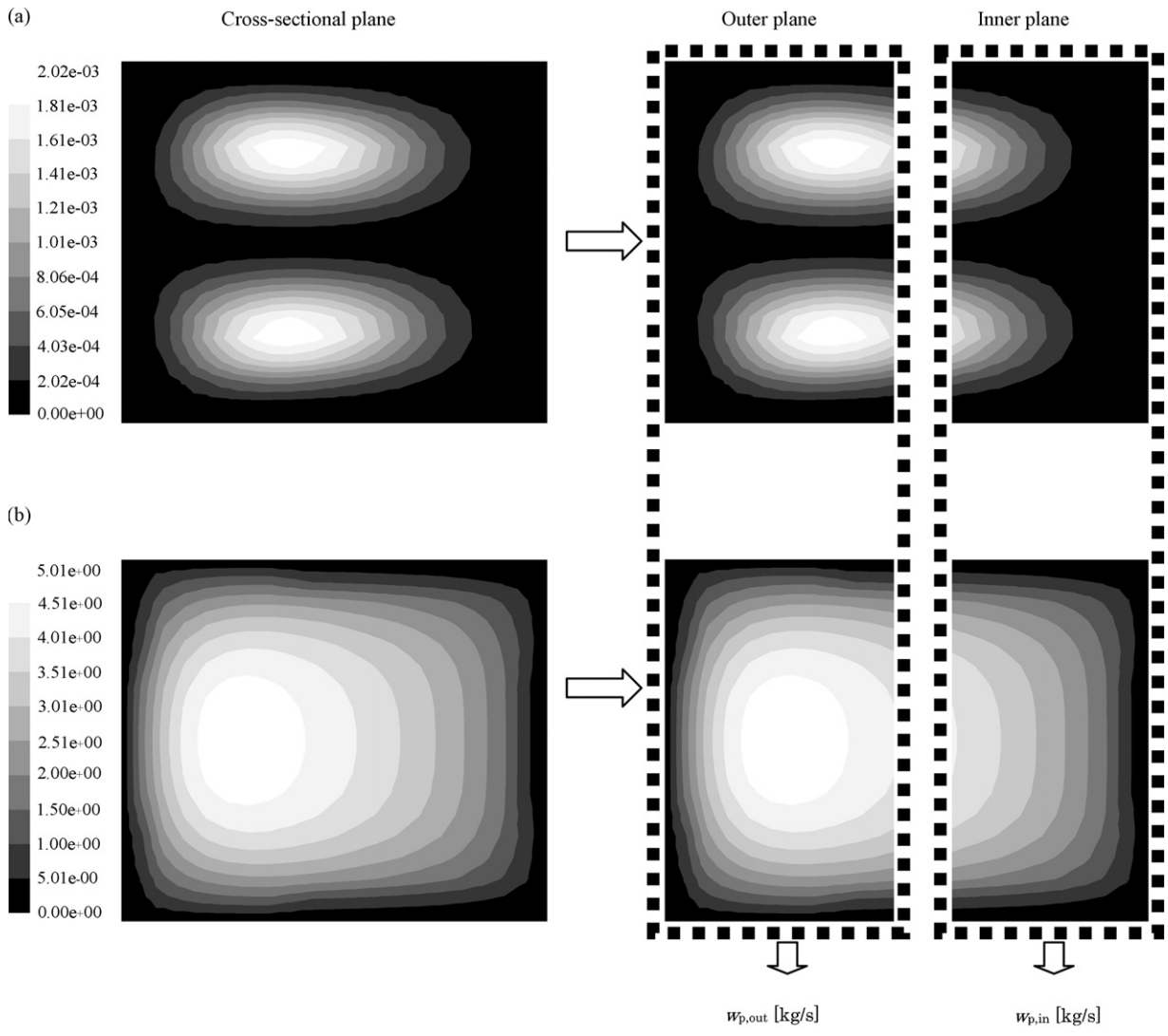

Fig. 3. Particulate (a) volume fraction (–) and (b) axial velocity (m/s) profiles at the arc end ($Re = 450$, $d_p = 10\,\mu m$).

at the downstream of the arc channel. The representative shear rate S is also defined based on the flow properties in the main channel. By using an equivalent diameter D_h and mean velocity U of the main channel, the S is defined as

$$S = \frac{8U}{D_h} \tag{20}$$

Although this expression gives a shear rate on the wall in laminar flow conditions for a circular pipe, it is conveniently adopted for the rectangular channel. Since the center of a particle cannot reach the wall surface, the particle cannot be exposed to the wall shear rate, which is highest in the channel. However, the extremely large centrifugal force shifts the highest velocity region outwards as seen in Fig. 3. As a result, the shear rates near the outer wall become much higher than values in the corresponding region of a straight channel. Therefore, even at the edge of concentrated region, it can be assumed that the shear rate would reach the value given by Eq. (20). It is noted that the S can be calculated based on the experimental conditions.

3. Results and discussion

The arc-end plane is divided into inner and outer planes at three representative positions so that the area ratio of outer to whole planes becomes (a) 0.4, (b) 0.5 and (c) 0.6, respectively. Figs. 4 and 5 show particle concentration profiles with the defined split positions indicated by white lines for given feed concentrations of 10 and 20 μm particles.

Fig. 6 is a color bar for these contour maps, in which the maximum concentration varies as (i) 0.0020, (ii) 0.058, (iii) 0.19 and (iv) 0.25 for Fig. 4 while (i) 0.0065, (ii) 0.0099, (iii) 0.059 and (iv) 0.087 for Fig. 5, respectively. Consequently, each ratio of maximum to feed concentrations C^* is (i) 3.3, (ii) 2.9, (iii) 1.9 and (iv) 1.7 in Fig. 4 while (i) 10.8, (ii) 9.9, (iii) 5.9 and (iv) 4.4 in Fig. 5, respectively. The minimum concentration is always zero except Fig. 4 (iv), in which the value is 9.9×10^{-5}.

As seen in Figs. 4 and 5, the concentration profiles do not significantly change in the dilute conditions, whose limits are (ii) $\alpha_{p,feed} = 0.02$ for 10 μm particles and (ii) $\alpha_{p,feed} = 0.001$ for

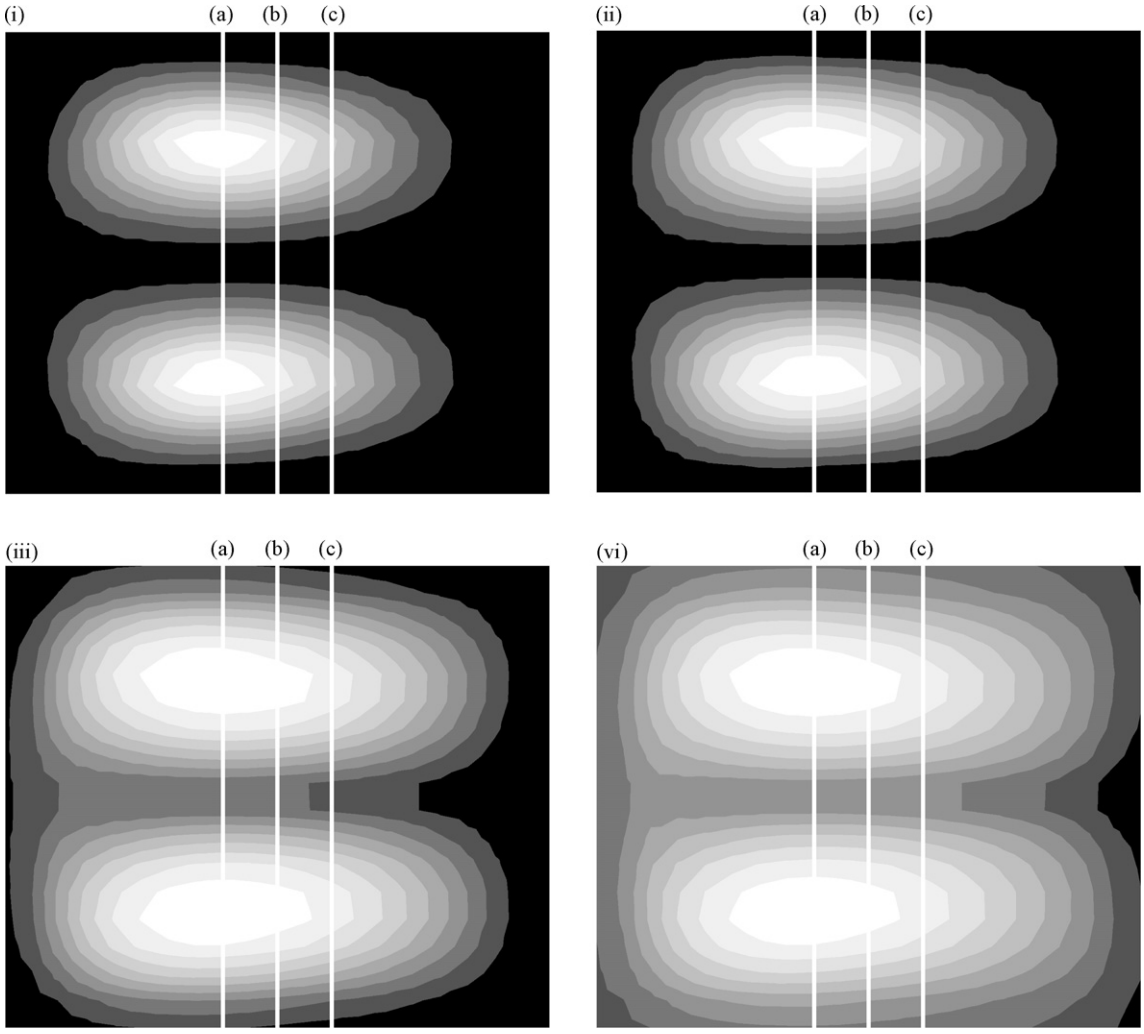

Fig. 4. Concentration profiles of 10 μm particles over the arc-end plane obtained at given feed concentrations. White lines indicate split positions so that the area ratio of outer (left in the figure) to whole planes becomes (a) 0.4, (b) 0.5 and (c) 0.6, respectively. (i) $\alpha_{p,feed} = 0.0006$; (ii) $\alpha_{p,feed} = 0.02$; (iii) $\alpha_{p,feed} = 0.10$; (iv) $\alpha_{p,feed} = 0.15$.

20 μm particles, respectively. In addition, the C^* is kept nearly highest for each particle size. It can be easily expected that the reduced particle recovery R_c remains constant regardless of the split position in such dilute conditions. Once the feed concentration exceeds the each limit, on the other hand, the concentrated region starts expanding along with the decline of the C^*. For 10 μm particles, all the split positions always exist in the expanding concentrated region. For 20 μm particles, on the other hand, it is expected that the split position much affects the relation between feed concentration and R_c. At the split position (a), the relation might be similar with the cases of 10 μm particles since the position always exists in the concentrated region. At the positions of (c), to the contrary, the R_c would remain higher since the most particles would still report to the outer plane even in the denser range.

Fig. 7 shows the relation between the *macroscopic* Stk_s and the R_c normalized by $R_{c,dilute}$ obtained at the most dilute condition, viz., $\alpha_{p,feed}$ of 0.0006. Each value beneath a group of plots indicates $\alpha_{p,feed}$ in [%]. For 10 μm particles, it can be seen that the split position does not largely affect the relation between the Stk_s and the normalized R_c, which clearly declines beyond the Stk_s of 0.1. It should be mentioned here that the C_e also declined beyond the $Stk_{s,micro}$ of 0.1 in spite those indices were based on local properties obtained at a point somewhere over the arc-end plane. It will be convenient that the same threshold is obtained from both the microscopic and *macroscopic* viewpoints. For 20 μm particles, on the other hand, the declining tendency of the normalized R_c depends on the split position. At position (a), the normalized R_c declines beyond the Stk_s of 0.1 similarly with 10 μm particles as expected. Then, the declining slope becomes smaller as the position shifts inwards from (b) to (c). This is apparently because the concentrated region mostly exists at outside of the split positions even in the denser conditions. Although the increase of feed concentration causes the expansion of the concentrated region, most particles are still recovered from the outer plane.

In the dilute range, the distance between the split position and the concentrated region can be regarded as a margin of the separation efficiency. If there exists a distance, then almost all the particles are recovered from the outer branch, viz., the R_c is practically unity. As the margin becomes smaller, the particle concentration in the outer branch preferably becomes larger with

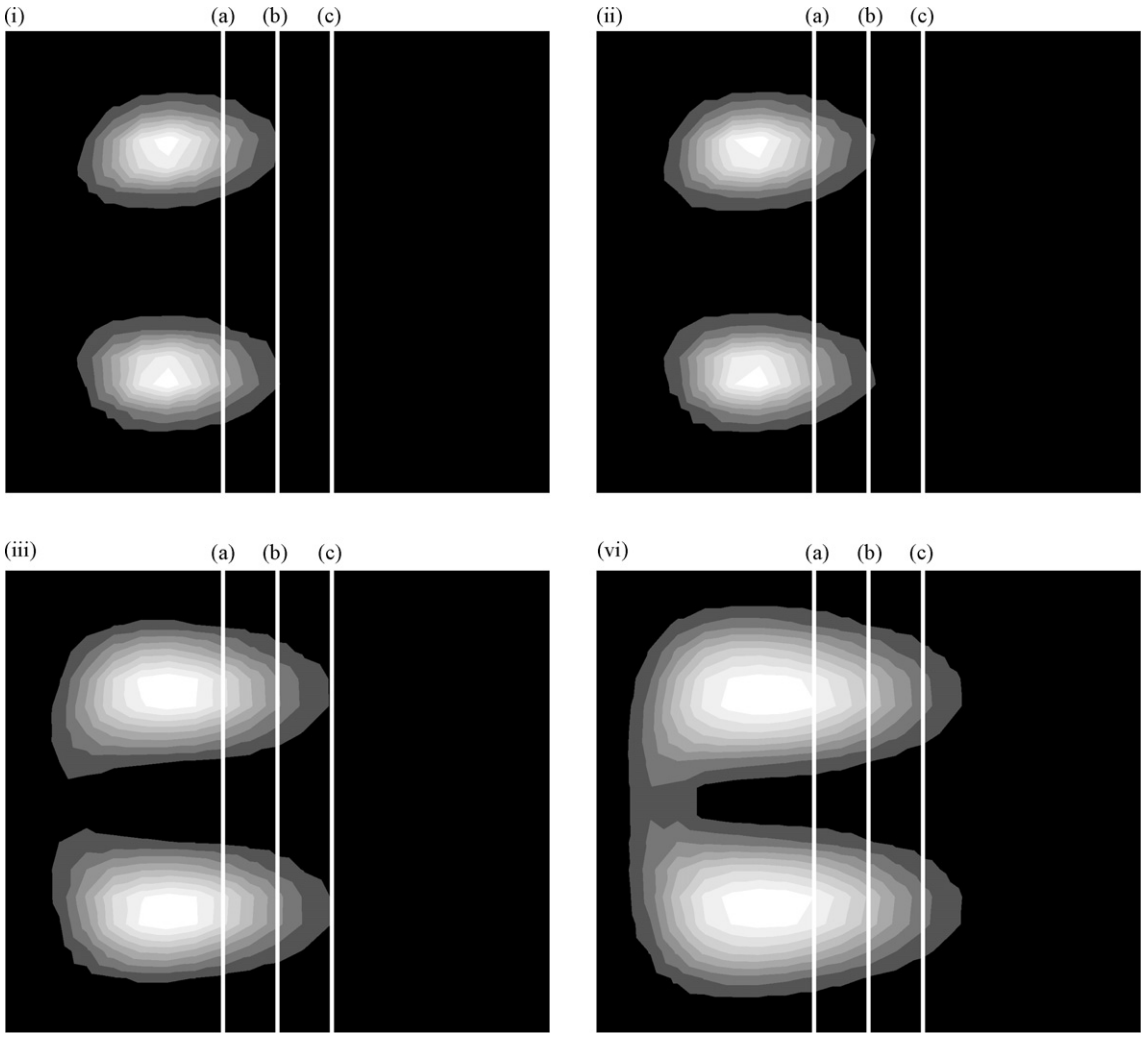

Fig. 5. Concentration profiles of 20 μm particles over the arc-end plane obtained at given feed concentrations. White lines indicate split positions so that the area ratio of outer (left in the figure) to whole planes becomes (a) 0.4, (b) 0.5 and (c) 0.6, respectively. (i) $\alpha_{p,feed} = 0.0006$; (ii) $\alpha_{p,feed} = 0.001$; (iii) $\alpha_{p,feed} = 0.01$; (iv) $\alpha_{p,feed} = 0.02$.

the highest R_c. That is, the efficiency becomes higher in terms of the slurry concentration as the split position shifts outward. If the normalized R_c remains high in the Stk_s range of above 0.1, therefore, one can know that the slurry concentration in the outer branch can be increased without the decline of R_c by decreasing the outer flow-rate but keeping total flow-rate constant.

Based on the better understanding of the characteristics of R_c, in conclusion, the operation of the micro-separator/classifier might be optimized as follows. At first, the device performance should be measured in the dilute Stk_s range of less than 0.01, where the normalized R_c sufficiently remains unity regardless of particle size and split position. It should be then examined whether the normalized R_c clearly declines in the Stk_s range of above 0.1. If the decline is observed, it is suggested that the split position exists within the concentrated region. Then, the device should be operated at a feed concentration to cause the Stk_s of 0.1. If the decline is not observed, it implies that there exits a margin between concentrated region and split position. In this case, the outer flow-rate should be decreased with keeping the R_c practically unity. The adjustment corresponds to shifting the split position outwards so that the margin becomes a minimum. After the adjustment, then, the device would be operated at Stk_s of 0.1. It should be mentioned that the optimized feed concentration here depends on the particle size as seen in Fig. 7. For the given Re condition, the $\alpha_{p,feed}$ of 0.035 and 0.005 would be the optimized feed concentrations for 10 and 20 μm particles, respectively. It can be concluded, therefore, that the Stk_s is useful for predicting a maximum feed concentration to be handled with a highest R_c for the particle size. It is noted that the highest R_c depends on particle size due to the concentration profile at the arc end.

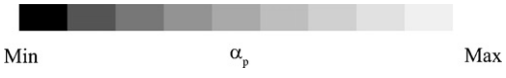

Fig. 6. Color bar for the contour maps.

In this study, the optimization procedure is discussed keeping total flow-rate, viz., Reynolds number Re constant in the main arc channel. It would be much difficult to optimize the operational conditions provided that the Re can be altered to

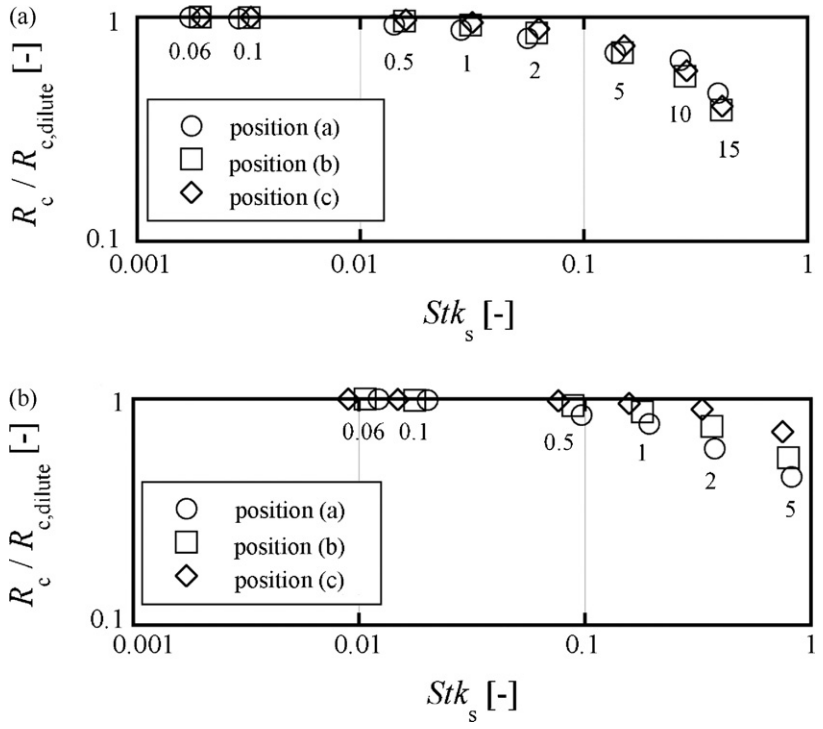

Fig. 7. The normalized separation efficiency $R_c/R_{c,dilute}$ with various flow split positions and Stk_s ($Re = 450$): (a) 10 μm particles; (b) 20 μm particles.

change the efficiency. Such ultimate optimization will be a future work based on the experimental work under progress. It is noted here that the trend seen in the numerical results qualitatively agrees with the experiments that will be soon reported elsewhere.

4. Conclusions

In the present numerical study, a *macroscopic* Stokes number Stk_s is newly proposed for the efficient operation of the micro-separator/classifier. It is shown that the Stk_s is useful to predict a maximum feed concentration to be handled with a highest reduced particle recovery R_c regardless of particle size at a given Reynolds number Re. The Stk_s of 0.1 is a threshold to give the maximum feed concentration with the highest R_c, both of which would vary according to particle size. The Stk_s is also useful to increase the device efficiency in terms of particle concentration in the outer branch at a given Re. The flow rate in the outer branch is to be decreased so that the normalized R_c clearly declines beyond the Stk_s of 0.1. It is important that both the Stk_s and R_c can be obtained in practical operations.

The usefulness of the novel Stk_s will be validated based on experiments under progress, which will be soon reported elsewhere. It is here noted that the trend seen in numerical results qualitatively agrees with the experiments. In the particle concentration profiles, the effect of gravity cannot be seen. It implies that the direction of the device does not affect the performance. For the optimized operation of the device, further, the effect of Re on the R_c should be considered, which makes the optimization complicated. It will be of further interest to examine these issues in future.

Acknowledgements

This research was partially supported by a Grant-in-Aid for Scientific Research (A) (No. 17206079) from Japan Society for the Promotion of Science (JSPS).

References

[1] S. Ookawara, R. Higashi, K. Ogawa, D. Street, Feasibility study on concentration of slurry and classification of contained particles by microchannel, in: Proceedings of the IMRET7, Lausanne, Switzerland, 2003, pp. 231–233.
[2] S. Ookawara, R. Higashi, D. Street, K. Ogawa, Feasibility study on concentration of slurry and classification of contained particles by microchannel, Chem. Eng. J. 101 (2004) 171–178.
[3] S. Ookawara, D. Street, K. Ogawa, A practical application of the Euler-granular model to a micro-separator/classifier, in: Proceedings of the International Conference on Multiphase Flow 2004, Yokohama, Japan, 2004 (Paper # 206).
[4] S. Ookawara, N. Oozeki, K. Ogawa, Experimental benchmark of a metallic micro-separator/classifier compared with representative hydrocyclone, in: Proceedings of the IMRET8, AIChE 2005 Spring National Meeting, Atlanta, GA, USA, 2005, p. 129g.
[5] S. Ookawara, D. Street, K. Ogawa, Quantitative prediction of separation efficiency of a micro-separator/classifier by an Euler-granular model, in: Proceedings of the IMRET8, AIChE 2005 Spring National Meeting, Atlanta, GA, USA, 2005, p. 130c.
[6] S. Ookawara, D. Street, K. Ogawa, Numerical study on development of particle concentration profiles in a curved microchannel, Chem. Eng. Sci. 61 (2006) 3714–3724.
[7] S. Ookawara, T. Ishikawa, K. Ogawa, Applicability of a miniaturized micro-separator/classifier to oil–water separation, Chem. Eng. Technol. 30 (2007) 316–321.
[8] S. Ookawara, D. Street, K. Ogawa, Quasi-direct numerical simulation of lift force-induced particle separation in a curved microchannel by

use of a macroscopic particle model, Chem. Eng. Sci. 62 (2007) 2454–2465.
[9] S. Ookawara, M. Agrawal, D. Street, K. Ogawa, A numerical study of influence of particle density on lift force-induced separation in a micro-separator/classifier by macroscopic particle model, J. Chem. Eng. Jpn., in press.
[10] C. Crowe, M. Sommerfield, Y. Tsuji, Multiphase Flows with Droplets and Particles, CRC Press, USA, 1997.
[11] Y. Yamamoto, M. Potthoff, T. Tanaka, T. Kajishima, Y. Tsuji, Large eddy simulation of turbulent gas-particle flow in a vertical channel: effect of considering inter-particle collisions, J. Fluid Mech. 442 (2001) 303–334.
[12] Fluent Inc., FLUENT 6.1 User's Guide, 2003.
[13] D.A. Drew, R.T. Lahey Jr., Analytical Modeling of Multiphase Flow. Particulate Two-phase Flow, Butterworth-Heinemann, Boston, 1993, pp. 509–566.
[14] P.G. Saffman, The lift on a small sphere in a slow shear flow, J. Fluid Mech. 22 (1965) 385–400.
[15] M. Syamlal, W. Rogers, T.J. O'Brien, NFX Documentation: Theory Guide, National Technical Information Service, Springfield, VA, 1993 (DOE/METC-9411004, NTIS/DE9400087).
[16] S.A. Vasquez, V.A. Ivanov, A phase coupled method for solving multi-phase problems on unstructured meshes, in: Proceedings of the ASME FEDSM'00: ASME 2000 Fluids Engineering Division Summer Meeting, Boston, 2000.